COMMUNICATION

Host-guest Interaction Modulation in Porous Coordination Polymers for Inverse Selective CO_2/C_2H_2 Separation

Yifan Gu [a,b], Jia-Jia Zheng [b,c], Ken-ichi Otake [b], Mohana Shivanna [b], Shigeyoshi Sakaki [c], Haruka Yoshino [d], Masaaki Ohba [d], Shogo Kawaguchi [e], Ying Wang [a], Fengting Li*[a], Susumu Kitagawa*[b]

[a] Dr. Y. Gu, Prof. Y. Wang, Prof. F. Li
College of Environmental Science and Engineering, Shanghai Institute of Pollution Control and Ecological Security, State Key Laboratory of Pollution Control and Resource Reuse, Tongji University.
Siping Rd 1239, 200092 Shanghai, China.
E-mail: fengting@tongji.edu.cn

[b] Dr. Y. Gu, Prof. J. Zheng, Prof. K. Otake, Dr.M. Shivanna, Prof. S. Kitagawa
Institute for Integrated Cell-Material Sciences, Kyoto University Institute for Advanced Study, Kyoto University, Yoshida Ushinomiya-cho, Sakyo-ku, Kyoto 606-8501, Japan.
E-mail: kitagawa@icems.kyoto-u.ac.jp

[c] Prof. J. Zheng, Prof. S. Sakaki
Fukui Institute for Fundamental Chemistry, Kyoto University, Takano Nishihiraki-cho 34-4, Sakyo-ku, Kyoto 606-8103, Japan.

[d] Mr. H. Yoshino, Prof. M. Ohba
Department of Chemistry, Faculty of Science, Kyushu University, Motooka 744, Fukuoka 819-0395, Nishi-ku, Japan

[e] Dr. S. Kawaguchi
Japan Synchrotron Radiation Research Insitute (JASRI), SPring-8, 1-1-1 Kouto, Sayo-cho, Sayo-gun, Hyogo 679-5198, Japan

Supporting information for this article is given via a link at the end of the document.

Abstract: Controlling gas sorption by simple pore modification is important in molecular recognition and industrial separation processes. In particular, it is challenging to realize the inverse selectivity, which reduces the adsorption of a high-affinity gas and increases the adsorption of a low-affinity gas. Herein, an “opposite action” strategy is demonstrated for boosting CO_2/C_2H_2 selectivity in porous coordination polymers (PCPs). A precise steric design of channel pores using an amino group as an additional interacting site enabled the synergetic increase in CO_2 adsorption while suppressing the C_2H_2 adsorption. Based on this strategy, two new ultramicroporous PCP physisorbents that are isostructural were synthesised. They exhibited the highest CO_2 uptake and CO_2/C_2H_2 volume uptake ratio at 298 K. Origin of this specific selectivity was verified by detailed density functional theory calculations. The breakthrough separation performances with remarkable stability and recyclability of both the PCPs render them relevant materials for C_2H_2 purification from CO_2/C_2H_2 mixtures.

Adsorptive gas separation or purification plays a key role in industries.[1] A general adsorptive gas separation process involves passing a gaseous mixture through a fixed-bed adsorber to directly yield a weakly adsorbed gaseous product. The strongly adsorbed component is recovered later at the desorption stage. However, harvesting high-purity products in the desorption stage is much more energy consuming (~40%) than directly collecting the gases that pass through without being adsorbed.[2] To recover the desorbed products, the use of multiple beds involving several steps is essential so that products with the desired purity can be obtained in the final step by counter-current vacuum blowdown.[3] Therefore, to make the adsorptive gas separation technologies more energy and process efficient, a "reverse selective separation" method is highly desirable in practical applications.[2a] This allows the gas to pass through the adsorbent even if the interaction force of the required gas is stronger than that of the partner gas. This strategy is vital for C_2H_2 purification from C_2H_2/CO_2 mixtures. C_2H_2, a key fuel and an essential feedstock for various industrial materials[4], is mainly produced via natural gas combustion or hydrocarbon cracking with CO_2 as a major impurity[5]. The separation of C_2H_2 and CO_2 is difficult due to their highly similar molecular size, shape, and boiling points (Table S1).[6] However, the higher quadrupole moment of C_2H_2 (7.2×10^{-26} esu cm^2) compared to that of CO_2 (0.65×10^{-26} esu cm^2) results in stronger electrostatic interaction of C_2H_2 with the sorbent, causing preferential adsorption over CO_2.[7] Thus, to avoid the usual energy-intensive desorption process to obtain pure C_2H_2, this study aims to design porous materials with inverse selectivity to achieve an effective one-step C_2H_2 purification method (Figure S1).

Porous coordination polymers (PCPs) or metal-organic frameworks (MOFs) are intriguing porous crystalline materials that allow the tailoring of pore sizes and functionalities suitable for the separation of a target species from a mixture.[8] Owing to the stronger interactions of C_2H_2 with a sorbent, it has been possible to synthesise a number of PCPs that have a higher affinity towards C_2H_2 than towards CO_2.[9] However, the aspect of inverse selectivity is still elusive, since there are rare adsorbents that favour the uptake of CO_2 over C_2H_2, especially at room temperature, although pore environment adjustment such as encoding functional groups and adjustable pore size has been well established for improving CO_2 selective adsorption.[7, 10] It is quite challenging to manipulate the pore chemistry to realise inverse selectivity, which suppresses the adsorption of the high-affinity adsorbate, C_2H_2, and increases the adsorption of the less affinity adsorbate, CO_2. An alternative strategy is the utilisation of the strong chemisorption of CO_2 endowed by -OH groups present in the pores of the PCPs. However, the regeneration process is more energy consuming.[10a, 10d] Therefore, there are several aspects that must be considered while attempting to design pores with actual inverse affinity: (I) selectivity for both adsorption and desorption without excess energy consumption, (II) excellent inverse selective separation performance at ambient condition, (III) enough stability and efficient adsorbent regeneration for

practical applications.[2a, 10a,d,e] Currently, there are still no well-defined strategies for constructing pores with such ideal inverse selectivity.

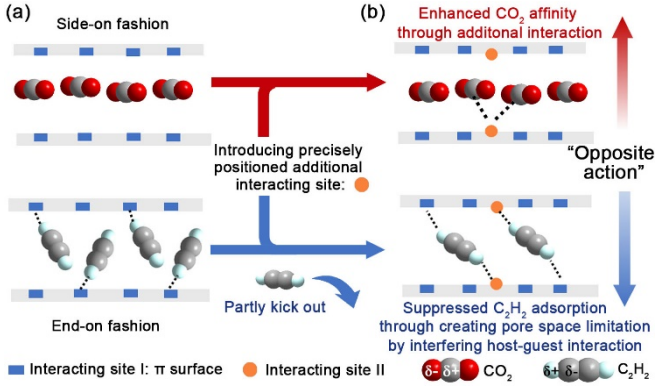

Scheme 1. Schematic illustration of the "opposite action" strategy for boosting CO_2/C_2H_2 selectivity. (a) Different binding modes of CO_2 and C_2H_2 in microporous channels. (b) Additional interacting site is precisely introduced to not only provide enhanced CO_2-framework interaction but also to suppress C_2H_2 adsorption by driving out some of the initially adsorbed C_2H_2 molecules; the latter is driven by space limitations originating from the interference in the pore–guest interaction, resulting in high inverse selectivity.

Herein, we demonstrate an "opposite action" strategy for boosting CO_2/C_2H_2 selectivity; that is, synergically increasing CO_2 affinity and suppressing C_2H_2 adsorption through precise steric arrangement of interaction sites on the pore surface. CO_2 and C_2H_2 exhibit distinct binding modes in microporous channels owing to their different electronic structures (Scheme 1a). Normally, CO_2 is adsorbed in a side-on orientation that it is well-adapted to the channel's electrostatic potential field, while C_2H_2 is adsorbed in a side-on orientation pointing to the host binding site.[7b, 9c] Therefore, precisely positioned additional interacting sites parallel to CO_2 binding sites can allow enhanced CO_2-framework interactions without apparently changing the orientation of the gas molecules (Scheme 1b). At the same time, the additional interacting site suppresses C_2H_2 adsorption by changing the adsorption position, driving out some of the adsorbed C_2H_2 molecules. Driving out of the adsorbed molecules is driven by the space limitation, which originates due to the interfered interaction between the pores and guest molecules, thus resulting in high inverse CO_2/C_2H_2 selectivity. To implement this strategy, we designed two PCP isomers, $[Co(ipa)(dpg)]_n$ (PCP-ipa; ipa = isophthalic acid, dpg = meso-*α,β*-di(4-pyridyl) glycol) and $[Co(bdc)(dpg)]_n$ (PCP-bdc; bdc = terephthalic acid), with similar 1-D ultramicroporous channels. The C_2H_2 molecules are hydrogen-bonded with the uncoordinated O atoms in an end-on fashion in the channel, while CO_2 adopts a side-on binding mode along the channel direction. Consequently, as a proof of concept of the "opposite action" strategy for high inverse selectivity, amino moieties were rationally appended into the channel surface using amino-substituted phthalic acid ligands. The synthesised $[Co(NH_2\text{-bdc})(dpg)]_n$ (PCP-NH_2-bdc; NH_2-bdc = 2-aminoterephthalic acid) and $[Co(NH_2\text{-ipa})(dpg)]_n$ (PCP-NH_2-ipa; NH_2-ipa = 5-aminoisophthalic acid) exhibit large CO_2 uptake with a high CO_2/C_2H_2 uptake ratio, which can be considered as a new physisorbent with specific inverse selectively. The separation performances and the remarkable stability and recyclability confirmed their performance in the one-step purification of C_2H_2.

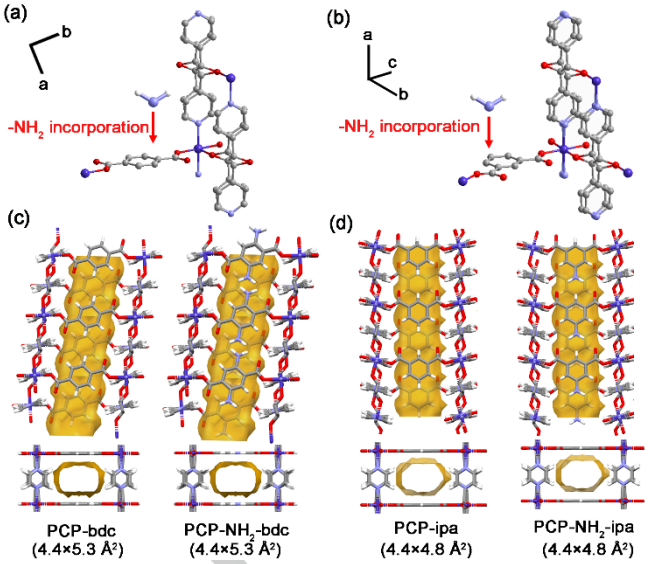

Figure 1. Crystal structures of PCP-bdc, PCP-ipa, PCP-NH_2-bdc, and PCP-NH_2-ipa. (a-b) Coordination environment of Co and amino group incorporated in PCP-bdc and PCP-ipa. (c-d) Ultramicroporous 1-D channels in PCP-bdc, PCP-ipa, PCP-NH_2-bdc, and PCP-NH_2-ipa. (Probe radius: 1.2 Å). Hydrogen atoms in the ligand backbones were fixed at their geometrically ideal positions. Purple, Red, blue, grey, and white colours in the PCP frameworks represent Co, N, C, and H, respectively.

Single crystals of PCP-bdc, PCP-ipa, PCP-NH_2-bdc, and PCP-NH_2-ipa[11] were synthesised via the solvothermal reaction of $Co(NO_3)_2{\cdot}6H_2O$, dpg, and NH_2-ipa or NH_2-bdc in mixed DMF/MeOH solutions (Figure S2-6). Single-crystal X-ray diffraction (SXRD) analysis revealed that PCP-ipa crystallises in the orthorhombic *Amm*2 space group and PCP-bdc crystallises in the triclinic $P\bar{1}$ space group (Table S2 and S3). In both PCP-ipa and PCP-bdc, the Co centre is six-coordinated in an octahedral geometry, coordinated by two N atoms from the pyridine ring, two O atoms from the hydroxyl group of the dpg ligand, and two O atoms from the carboxylic group of the phthalic acid ligands (Figure 1a and 1b). Interestingly, these two PCP isomers synthesised using isophthalic acid or terephthalic acid ligands exhibit analogous crystal structures owing to the similar coordination environment of Co, resulting in a similar narrow 1-D channel of the π ligand system (Figure 1c and 1d). Notably, the uncoordinated negatively charged O atoms from the ipa/bdc ligand are present on the 1-D ultramicroporous channels in both the PCPs. To engineer the channel surface for modulating the position for guest-binding, in this study, isostructural variants of PCP-bdc and PCP-ipa, i.e., PCP-NH_2-bdc and PCP-NH_2-ipa, were synthesised by incorporating amino groups into the bdc/ipa ligands (Figure 1a and 1b and Table S4 and S5). Pore size of these microporous channels was estimated to be 4.4×5.3 $Å^2$ for PCP-bdc and PCP-NH_2-bdc and 4.4×4.8 $Å^2$ for PCP-ipa and PCP-NH_2-ipa (Figure 1c and 1d) from their framework structure (probe radius: 1.2 Å). To confirm the valency of Co, PCP-NH_2-ipa and PCP-NH_2-bdc were selected for X-ray photoelectron spectroscopy and magnetic studies. The results consistently suggested that Co was divalent in both the PCPs (Figure S7-9). Phase purity of all the prepared PCPs was confirmed by comparing the simulated and experimental power X-ray diffraction (PXRD) patterns (Figure S10-S13). Thermogravimetric analysis (TGA) clearly showed that the guest molecules were completely

removed after activation. Moreover, the TGA revealed that the framework was thermally stable up to *ca.* 280 °C for all the PCPs (Figure S14-S17), indicating their good thermostability.

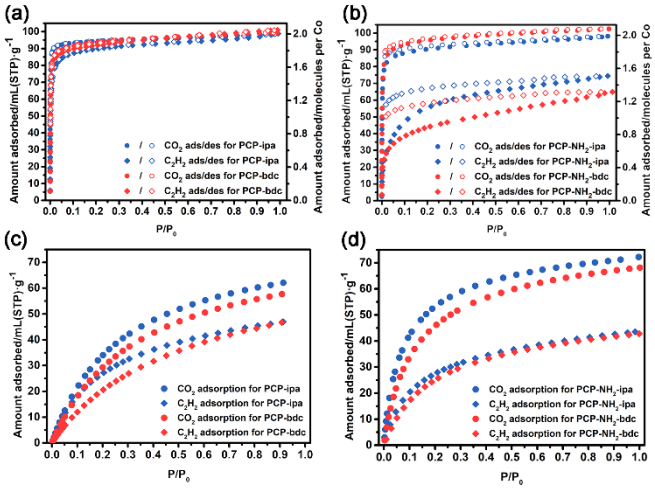

Figure 2. CO_2 and C_2H_2 sorption for PCP-ipa and PCP-bdc (a) and PCP-NH_2-ipa and PCP-NH_2-bdc (b) at 195 K. CO_2 and C_2H_2 adsorption for PCP-ipa and PCP-bdc (c) and PCP-NH_2-ipa and PCP-NH_2-bdc (d) at 298 K.

The adsorption isotherms of C_2H_2 and CO_2 were first collected at 195 K. As shown in Figure 2a, PCP-ipa and PCP-bdc exhibit similar type I CO_2 and C_2H_2 sorption isotherms at 195 K, corresponding to the same saturated uptake amount (~2 molecules per Co^{2+}) for both the gases. Notably, after encoding the -NH_2 group, C_2H_2 uptake at 195 K was found to be much lower than CO_2 uptake, indicating that there were lesser number of binding sites for C_2H_2 in PCP-NH_2-ipa and PCP-NH_2-bdc. Figure 2b shows that the maximum CO_2 uptake by PCP-NH_2-ipa and PCP-NH_2-bdc at 195 K was *ca.* 99 mL·g^{-1} and *ca.* 101 mL·g^{-1}, respectively, corresponding to ~2 molecules per Co^{2+} in both the PCPs. Meanwhile, the maximum C_2H_2 uptake was only *ca.* 74 mL·g^{-1} (~1.5 molecules per Co^{2+}) for PCP-NH_2-ipa and *ca.* 65 mL·g^{-1} (~1.4 molecules per Co^{2+}) for PCP-NH_2-bdc. In addition, the sharp rise in CO_2 uptake in the low pressure region of CO_2 indicates that both PCP-NH_2-ipa and PCP-NH_2-bdc exhibit higher affinity for CO_2 than for C_2H_2. Hence, distinct CO_2 and C_2H_2 adsorption modes are promoted by anchoring -NH_2 group into the channel surface. The CO_2 and C_2H_2 adsorption was also studied at ambient temperature. As shown in Figure 2c, PCP-ipa and PCP-bdc exhibit similar CO_2 and C_2H_2 adsorption at 298 K, indicating their comparable affinity towards CO_2 and C_2H_2. As expected, PCP-NH_2-ipa and PCP-NH_2-bdc show obvious preferential adsorption of CO_2 over C_2H_2 at 273, 298, and 313 K (Figure 2d and Figure S18-S21). Notably, the CO_2 uptake capacity and CO_2/C_2H_2 uptake ratio (v/v) of PCP-NH_2-ipa and PCP- NH_2-bdc are high at 298 K and 1 bar. PCP-NH_2-ipa exhibits a maximum CO_2 uptake of *ca.* 72 mL·g^{-1} (3.21 mmol·g^{-1}) and a CO_2/C_2H_2 uptake ratio of 1.66 (Figure 2d). For PCP-NH_2-bdc, the CO_2 uptake capacity was *ca.* 68 mL·g^{-1} (3.03 mmol·g^{-1}) and the CO_2/C_2H_2 uptake ratio was 1.59. The CO_2 uptake and CO_2/C_2H_2 uptake ratio of both the PCPs are higher than those of the reported PCP physisorbents such as SIFSIX-3-Ni[10e], NbOFFIVE-1-Ni[10c] and AlFFIVE-1-Ni[10c], which show inverse adsorption ability under similar conditions (Figure 3a). In addition, no apparent decrease in the CO_2 uptake capacity was observed after five cycles at 298 K, implying good regeneration abilities of both the PCPs for CO_2 adsorption (Figure S22). These gas sorption results demonstrate that PCP-NH_2-ipa and PCP-NH_2-bdc are potential candidates for trapping CO_2 from CO_2/C_2H_2 gas mixture.

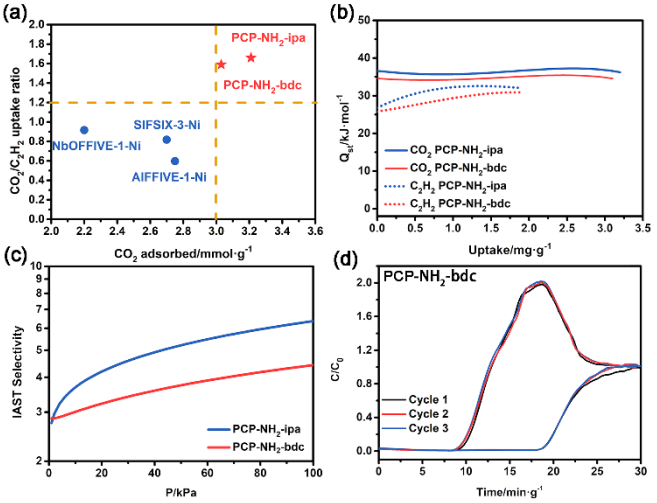

Figure 3. (a) CO_2 uptake amount and CO_2/C_2H_2 uptake ratio of the representative PCP physisorbents with inverse selectivity for CO_2/C_2H_2 separation at 1 bar and 298 K. (b) Isosteric heats of adsorption (*Qst*) for CO_2 and C_2H_2. (c) IAST selectivity of PCP-NH_2-ipa and PCP-NH_2-bdc for CO_2/C_2H_2 (v/v, 50/50) at 298 K. (d) Three cycles of experimental breakthrough curve of PCP-NH_2-bdc at a flow rate at 4 mL/min for an equimolar gaseous mixture of C_2H_2 and CO_2 (v/v, 50/50) at room temperature. Between each cycle, the PCPs were regenerated by *in situ* vacuuming without heating.

The isosteric heat of adsorption (*Qst*) is used to evaluate the strength of interaction between the PCPs and CO_2 or C_2H_2 and was calculated from the adsorption isotherms recorded at 273, 298, and 313 K (Table S6). As shown in Figure 3b, the *Qst* values of CO_2 at near-zero coverage on PCP-NH_2-ipa and PCP-NH_2-bdc are 36.6 and 34.57 kJ·mol^{-1}, respectively. Notably, these values are lower than that of SIFSIX-3-Ni (50.9 kJ·mol^{-1})[10e], NbOFFIVE-1-Ni (54.6 kJ·mol^{-1})[12], AlFFIVE-1-Ni (47.0 kJ·mol^{-1})[12], CD-MOF-1 (41.0 kJ·mol^{-1})[10d], and CD-MOF-2 (46.3 kJ·mol^{-1})[10d]. These values indicate that the desorption process by PCP-NH_2-ipa and PCP-NH_2-bdc is less energy consuming compared to the previously reported PCP adsorbents, and this would be beneficial for practical applications.[12] For comparison, the *Qst* values of C_2H_2 at near-zero coverage on PCP-NH_2-ipa and PCP-NH_2-bdc are only 26.8 and 25.6 kJ·mol^{-1}, respectively. These are much lower than those for CO_2, implying the weaker interaction between C_2H_2 and the PCP frameworks. To further predict the selectivity towards a CO_2/C_2H_2 binary mixture for separation in practical applications, the ideal adsorbed solution theory (IAST) was used. As shown in Figure 3c, the IAST selectivities of PCP-NH_2-ipa and PCP-NH_2-bdc for an equimolar mixture of CO_2/C_2H_2 at 298 K and 1 bar were up to 6.4 and 4.4, respectively. Notably, the IAST selectivity of PCP-NH_2-ipa can be comparable with SIFSIX-3-Ni[10e] (6.95 for an equimolar mixture of CO_2/C_2H_2 at 298 K and 1 bar) as current highest one as physisorbents, but lower than $[Tm_2(OH\text{-}bdc)_2(\mu3\text{-}OH)_2(H_2O)_2]$ [10a] [17.5 for CO_2/C_2H_2 (1/2; V/V) at 298 K and 1 bar] in which chemisorption of CO_2 was observed. The large difference between the isosteric heat of adsorption for CO_2 and C_2H_2 and the high IAST selectivity indicate the promising potential of both the PCPs for the separation of CO_2/C_2H_2 binary mixture under dynamic conditions.

To further evaluate the practical C_2H_2/CO_2 separation performance of both the PCPs, we conducted breakthrough tests under room temperatures (Figure S23). A mixture of C_2H_2/CO_2 (50:50, v/v) at a flow rate of 4 mL/min was passed through a fixed-bed column filled with PCP-NH_2-ipa or PCP-NH_2-bdc. Remarkable one-step C_2H_2 purification performance was achieved with both the PCPs (Figure 3d and S24). C_2H_2 (purity> 99.5%) was first eluted from the separation bed at about 8 min·g^{-1} for PCP-NH_2-bdc and 10 min·g^{-1} for PCP-NH_2-ipa, while CO_2 was captured as an impurity in a packed column until its saturated uptake (Figure S25). The breakthrough time is 11 min·g^{-1} for both the PCPs. Based on the results of binary breakthrough experiments, the C_2H_2 productivity was calculated as 0.98 mol·g^{-1} for both PCP-NH_2-ipa and PCP-NH_2-bdc. An ideal adsorbent for practical applications should have good recyclability and an energy-efficient regeneration process. Thus, we performed cycling breakthrough experiments under the same conditions. Between each cycle, the PCPs were regenerated by *in situ* vacuuming without heating. The results showed that both the PCPs maintain the same retention time and C_2H_2 productivity. Moreover, after the breakthrough cycling test, both the PCPs retained their crystal structures (Figure S26 and S27). In addition, both the PCPs show excellent water stability. The crystallinities of both the PCPs were unaffected even after soaking them directly in water for 3 days (Figure S28 and S29). Moreover, after the water stability tests, the CO_2 sorption performance of both the PCPs at 298 K was same as that of the pristine samples (Figure S30 and S31). The good stability properties are conducive for practical applications.

To further verify the "opposite action" strategy for boosting CO_2/C_2H_2 selectivity, we conducted theoretical calculations of CO_2 and C_2H_2 adsorption into PCP-NH_2-bdc and PCP-bdc. The adsorption structures of CO_2 and C_2H_2 (Figure 4) in these two PCPs were obtained by classical Monte Carlo simulation[13], followed by geometry optimisation using periodic density functional theory calculation with the PBE-D3 functional[14] (see supporting information for computational details). In the case of CO_2, both PCP-NH_2-bdc and PCP-bdc have two kinds of adsorption sites (sites I and II in Figure 4a and 4b), each of which is located at four equivalent position in one unit cell; this results in the adsorption of 2 CO_2 molecules per Co^{2+}. When all these adsorption sites are occupied by CO_2 molecules, the bonding energy (BE) per CO_2 molecule is −10.3 and −9.2 kcal/mol for PCP-NH_2-bdc and PCP-bdc, respectively, indicating that PCP-NH_2-bdc has a stronger affinity towards CO_2 compared to PCP-bdc. This enhanced affinity of PCP-NH_2-bdc for CO_2 arises from the presence of the -NH_2 group, which allows additional interaction with CO_2 [site I, $C^{(\delta+)}\cdots N^{(\delta-)}$ = 3.436 Å; site II, $C^{(\delta+)}\cdots N^{(\delta-)}$ = 3.591 Å, Figure 4a]. This induces stronger electrostatic interaction of CO_2 with PCP-NH_2-bdc than with PCP-bdc (Table S7).

On the other hand, PCP-NH_2-bdc shows suppressed C_2H_2 adsorption (Figure 4c and 4d) while it adsorbs only 6 C_2H_2 molecules in one unit cell (1.5 C_2H_2/Co^{2+}), PCP-bdc adsorbs 8 C_2H_2 molecules in one unit cell (2 C_2H_2/Co^{2+}). We, therefore, focus on the adsorption structures with 6 and 8 C_2H_2 molecules in one unit cell of PCP-NH_2-bdc and PCP-bdc. In PCP-NH_2-bdc, the calculated BE is −8.7 kcal/mol per molecule for the adsorption of 8 C_2H_2 molecules and −9.6 kcal/mol for the adsorption of 6 C_2H_2 molecules, indicating that the average BE for adsorption of the 7th and 8th C_2H_2 molecules is −6.0 kcal/mol. Because this BE for the adsorption of the 7th and 8th C_2H_2 molecules is too small to compensate for the entropy decrease due to C_2H_2 adsorption ($\Delta G°$= −0.1 kcal/mol), the 7th and 8th C_2H_2 molecules cannot be adsorbed in PCP-NH_2-bdc. In the case of PCP-bdc, the BEs for the adsorption of 6 and 8 C_2H_2 molecules in one cell are −9.6 and −9.2 kcal/mol, respectively, indicating that the BE for the adsorption of the 7th and 8th C_2H_2 molecules is almost same as that of the first six C_2H_2 molecules ($\Delta G°$= −1.5 kcal/mol). These results lead to the conclusion that a total of 8 C_2H_2 molecules can be adsorbed in one unit cell of PCP-bdc at the saturation limit, but only 6 C_2H_2 molecules can be adsorbed in one unit cell of PCP-NH_2-bdc. This is consistent with the experimentally determined saturated C_2H_2 adsorption amounts in these two PCPs.

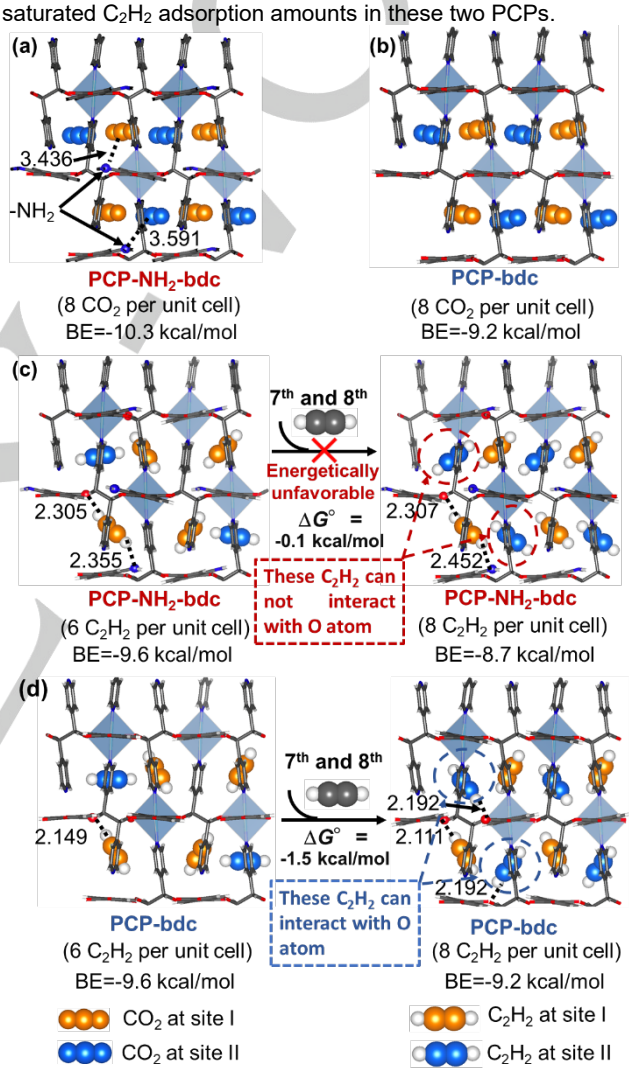

Figure 4. Calculated CO_2 (a-b) and C_2H_2 (c-d) adsorption structures in PCP-NH_2-bdc and PCP-bdc, showing two kinds of adsorption sites. Orientation of the C_2H_2 molecule is slightly different in sites I and II at different loading. Distances are given in Å. Red, blue, grey, and white colours in the PCP frameworks represent O, N, C, and H, respectively.

We further investigated the C_2H_2 adsorption structures to understand the reason for the suppressed C_2H_2 adsorption in PCP-NH_2-bdc. In the case of PCP-bdc, the H atoms of all the C_2H_2 molecules interact with the negatively charged O atoms of the bdc ligand through hydrogen bonding interactions (site I: C-H···O =

2.111 Å, site II: C-H···O = 2.192 Å). However, in PCP-NH_2-bdc, the orientation of the C_2H_2 molecule at site I is different from that in PCP-bdc because it forms hydrogen bonding interactions with both O and NH_2 group of NH_2-bdc ligand (C-H···N = 2.355 Å; C-H···O = 2.305 Å). This change in orientation further prevents the next C_2H_2 molecules (site II) occupying the optimum position for hydrogen bonding interaction with the O atom of NH_2-bdc ligand. In other words, C_2H_2 at site II forms hydrogen bond with O of the bdc ligands in PCP-bdc but not in PCP-NH_2-bdc. It is concluded that the orientation of C_2H_2 at site I changes in PCP-NH_2-bdc due to hydrogen bonding interaction with the O atom and NH_2 group of NH_2-bdc, thereby suppressing the C_2H_2 adsorption at site II by interfering in the adsorption position at site II by interfering in the adsorption position; it is worth noting that 1-D confined channel of this PCP does not provide enough space to the adsorbed molecule. For CO_2 adsorption, the introduced -NH_2 group does not apparently change the orientation of the adsorbed CO_2 molecules because the position of the -NH_2 group is parallel to that of the CO_2 molecules (Figure 4a and 4b). Moreover, it enhances CO_2-framework interactions, as discussed above, resulting in a stronger adsorption affinity for CO_2 than for C_2H_2. These results verify our “opposite action” strategy for boosting inverse selectivity.

It has been shown that gas species that are difficult to separate using conventional methods can be separated using PCP/MOF even if the gas species are very similar in size and shape, by taking advantage of the slight difference in the interaction forces. However, when the objective is to purify a high-affinity gas, it is practically desirable to preferentially capture the weak-affinity gas and allow the high-affinity gas to pass through. Nonetheless, precise designing of porous materials with ideal inverse selectivity to meet such separation requirements remains a formidable task. In this study, we focused on the differences in the electronic structure of the target gases and succeeded in generating the opposite selectivity by steric control of the pore surface and guest gas interaction in the PCP pores. This “opposite action” strategy may be broadly applicable to other gas systems and offers a promising design principle for porous materials with high performance for challenging recognition and separation systems.

Acknowledgements

This work was supported by the National Natural Science Foundation of China (21906120, 51978491) and a KAKENHI Grant-in-Aid for Scientific Research (S) (JP18H05262), Early-Career Scientists (JP19K15584) from the Japan Society for the Promotion of Science (JSPS). Synchrotron SXRD measurements were supported by the Japan Synchrotron Radiation Research Institute (JASRI) (Proposal Nos. 2019B1296, 2019A1136, 2020A1412, 2020A0617). We thank Ms. Nanae Shimanaka for assistance with X-ray diffraction analysis.

Keywords: porous coordination polymers • CO_2/C_2H_2 separation • inverse selectivity • binding site control • ultramicroporous materials

[1] R. T. Yang, *Gas separation by adsorption processes, Vol. 1*, World Scientific, **1997**.

[2] a) L. Li, R.-B. Lin, R. Krishna, H. Li, S. Xiang, H. Wu, J. Li, W. Zhou, B. Chen, *Science* **2018**, *362*, 443-446; b) A. Mersmann, B. Fill, R. Hartmann, S. Maurer, *Chem. Eng. Technol.* **2000**, *23*, 937-944.

[3] a) F. A. D. Silva, A. E. Rodrigues, *AIChE J.* **2001**, *47*, 341-357; b) C. A. Grande, F. Poplow, A. E. Rodrigues, *Sep. Sci. Technol.* **2010**, *45*, 1252-1259; c) R. Krishna, *RSC adv.* **2015**, *5*, 52269-52295.

[4] Z. Zhang, S. B. Peh, Y. Wang, C. Kang, W. Fan, D. Zhao, *Angew. Chem. Int. Ed.* **2020**, *59*, 18927-18932.

[5] M. Bohnet, *Ullmann's encyclopedia of industrial chemistry*, Wiley-Vch, **2003**.

[6] C. Reid, K. Thomas, *J. Phy. Chem. B.* **2001**, *105*, 10619-10629.

[7] a) R. Eguchi, S. Uchida, N. Mizuno, *Angew. Chem. Int. Ed.* **2012**, *51*, 1635-1639; b) M. L. Foo, R. Matsuda, Y. Hijikata, R. Krishna, H. Sato, S. Horike, A. Hori, J. Duan, Y. Sato, Y. Kubota, M. Takata, S. Kitagawa, *J. Am. Chem. Soc.* **2016**, *138*, 3022-3030.

[8] a) J.-R. Li, R. J. Kuppler, H.-C. Zhou, *Chem. Soc. Rev.* **2009**, *38*, 1477-1504; b) R.-B. Lin, S. Xiang, W. Zhou, B. Chen, *Chem* **2020**, *6*, 337-363; c) J. Li, P. M. Bhatt, J. Li, M. Eddaoudi, Y. Liu, *Adv. Mater.* **2020**, 2002563; d) X. Zhao, Y. Wang, D.-S. Li, X. Bu, P. Feng, *Adv. Mater.* **2018**, *30*, 1705189; e) K. B. Idrees, Z. Chen, X. Zhang, M. R. Mian, R. J. Drout, T. Islamoglu, O. K. Farha, *Chem. Mater.* **2020**, *32*, 3776–3782; f) D.-D. Zhou, P. Chen, C. Wang, S.-S. Wang, Y. Du, H. Yan, Z.-M. Ye, C.-T. He, R.-K. Huang, Z.-W. Mo, N.-Y Huang, J.-P Zhang, *Nat. Mater.* **2019**, *18*, 994-998; g) Y. Yan, M. Juríček, F.-X. Coudert, N. A. Vermeulen, S. Grunder, A. Dailly, W. Lewis, A. J. Blake, J. F. Stoddart, M. Schröder, *J. Am. Chem. Soc.* **2016**, *138*, 3371-3381.

[9] a) W. Fan, S. Yuan, W. Wang, L. Feng, X. Liu, X. Zhang, X. Wang, Z. Kang, F. Dai, D. Yuan, D. Sun, H.-C. Zhou, *J. Am. Chem. Soc.* **2020**, *142*, 8728-8737; b) S. Mukherjee, D. Sensharma, K.-J. Chen, M. J. Zaworotko, *Chem. Commun.* **2020**, *56*, 10419-10441; c) R.-B. Lin, L. Li, H. Wu, H. Arman, B. Li, R.-G. Lin, W. Zhou, B. Chen, *J. Am. Chem. Soc.* **2017**, *139*, 8022-8028; d) H. Zeng, M. Xie, Y. L. Huang, Y. Zhao, X. J. Xie, J. P. Bai, M. Y. Wan, R. Krishna, W. Lu, D. Li, *Angew. Chem. Int. Ed.* **2019**, *58*, 8515-8519; e) L. Yang, L. Yan, Y. Wang, Z. Liu, J. He, Q. Fu, D. Liu, X. Gu, P. Dai, L. Li, X. Zhao, *Angew. Chem. Int. Ed.* **2020**, Doi: 10.1002/anie.202013965.

[10] a) D. Ma, Z. Li, J. Zhu, Y. Zhou, L. Chen, X. Mai, M. Liufu, Y. Wu, Y. Li, *J. Mater. Chem. A.* **2020**, *8*, 11933-11937; b) W. Yang, A. J. Davies, X. Lin, M. Suyetin, R. Matsuda, A. J. Blake, C. Wilson, W. Lewis, J. E. Parker, C. C. Tang, *Chem. Sci.* **2012**, *3*, 2993-2999; c) Y. Belmabkhout, Z. Zhang, K. Adil, P. M. Bhatt, A. Cadiau, V. Solovyeva, H. Xing, M. Eddaoudi, *Chem. Eng. J.* **2019**, *359*, 32-36; d) L. Li, J. Wang, Z. Zhang, Q. Yang, Y. Yang, B. Su, Z. Bao, Q. Ren, *Acs. Appl. Mater. Inter.* **2018**, *11*, 2543-2550; e) K.-J. Chen, H. S. Scott, D. G. Madden, T. Pham, A. Kumar, A. Bajpai, M. Lusi, K. A. Forrest, B. Space, J. J. Perry IV, M. J. Zaworotko, *Chem* **2016**, *1*, 753-765.

[11] Crystallographic data in CIF format have been deposited in the Cambridge Crystallographic Data Centre (CCDC) under deposition numbers: 2049879 (PCP-NH_2-bdc), 2049880 (PCP-NH_2-ipa), 2049881 (PCP-bdc), and 2050488 (PCP-ipa).

[12] W. Liang, P. M. Bhatt, A. Shkurenko, K. Adil, G. Mouchaham, H. Aggarwal, A. Mallick, A. Jamal, Y. Belmabkhout, M. Eddaoudi, *Chem* **2019**, *5*, 950-963.

[13] D. Frenkel, B. Smit, *Understanding Molecular Simulation*, Academic Press, San Diego, **2001**.

[14] S. Grimme, J. Antony, S. Ehrlich, H. Krieg, *J. Chem. Phys.* **2010**, *132*, 154104.

Entry for the Table of Contents

Insert graphic for Table of Contents here.

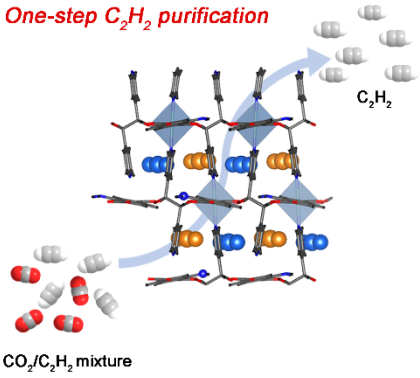

Boosting inverse CO_2/C_2H_2 selectivity is achieved through precise steric design of amino groups in the pore surface to provide enhanced CO_2-framework interactions and suppressed C_2H_2 adsorption. The obtained two new PCPs exhibit high CO_2 uptake and strong separation performance for one-step C_2H_2 purification at room temperature, which can be considered as new physisorbents with this specific inverse selectivity.